Environmental Science Nano

ROYAL SOCIETY OF CHEMISTRY

PAPER

View Article Online
View Journal | View Issue

Cite this: *Environ. Sci.: Nano*, 2025, **12**, 4069

Quantifying biolipid (rhamnolipid) effects on the aggregation behavior of engineered nanoparticles†

Anushree Ghosh, [ab] Neha Sharma,[c] Junseok Lee,[d] Wenlu Li,[e] Ji-Won Son,[f] Changwoo Kim, [f] Natalie L. Cápiro, [g] Kurt Pennell, [h] Kimberly M. Parker[b] and John D. Fortner [*a]

Predicting nanoscale material stability in aqueous systems is essential to accurately model particle fate and transport in the environment. Such stability is not only a function of particle surface chemistry and ionic strength and type, but can also be strongly affected by common aqueous constituents including natural organic matter (NOM), proteins, and lipids, among other macromolecules. Of these, biological surfactants, when present, have been hypothesized to play a significant, interfacial role with regard to nanoparticle stability, mobility and thus ultimate fate. Specifically, the role(s) of rhamnolipid(s), which are some of the most common naturally occurring biosurfactants, remains unclear. To address this knowledge gap, aggregation dynamics of 8 nm monodispersed iron oxide (nano)particles (IONPs) with cationic and anionic surface chemistries were evaluated in the presence of monorhamnolipid (monoRL) and dirhamnolipid (diRL), two amphiphilic glycolipids excreted by *Pseudomonas aeruginosa*, among other bacteria. Results demonstrate that IONP surface charge, RL type (*i.e.* mono- *vs.* dirhamnolipid), and concentration govern particle stability. Further, water chemistry (considering monovalent and divalent ions) plays a key role in these processes and outcomes. RLs at higher concentrations (above CMC_{monoRL} = 20.9, CMC_{diRL} = 10.1 mg of OC L^{-1}) adsorbed strongly on anionic IONPs. For these, the critical coagulation concentration (CCC) of anionic IONPs increased from 700 mM to 1500 mM in the presence of DiRL. RLs also strongly adsorb on IONP with a positive surface charge (at concentrations < CMC). Positively charged IONPs aggregated at intermediate concentrations (~CMC) of monoRL and diRL, and then effectively re-stabilized at higher concentrations (1.5–2 CMC) due to (NP) surface RL bilayer formation. For RL coated IONPs, three distinct aggregation regimes were identified as a function of electrolyte concentration (1–2000 mM), for which positively charged IONPs do not follow typical DLVO-based particle interaction theory.

Received 9th April 2025,
Accepted 17th June 2025

DOI: 10.1039/d5en00376h

rsc.li/es-nano

Environmental significance

This study systematically and quantitatively explores the influence of rhamnolipids (RL), specifically monorhamnolipid and dirhamnolipid biosurfactants, on the stability and aggregation dynamics of nanoscale (iron oxide) particles in aqueous systems, highlighting how (RL) adsorption behavior and concentration (thus RL surface grafting density and structure), along with ionic strength are critical and interrelated factors which strongly control particle behavior.

[a] *Department of Chemical and Environmental Engineering, Yale University, New Haven, CT 06520, USA. E-mail: john.fortner@yale.edu; Tel: +1 314 935 9293*
[b] *Department of Energy, Environmental and Chemical Engineering, Washington University in St. Louis, St. Louis, MO 63130, USA*
[c] *Department of Chemical Engineering, Stanford University, Stanford, CA, USA*
[d] *Department of Environmental Engineering, Incheon National University, 119 Academyro, Yeonsugu, Incheon, Korea*
[e] *School of Ecology and Environment, Northwestern Polytechnical University, Xi'an 710072, China*
[f] *Department of Environment and Energy Engineering, Gwangju Institute of Science and Technology, Gwangju, Korea*
[g] *Department of Biological & Environmental Engineering, Cornell University, Ithaca, NY 14853, USA*
[h] *School of Engineering, Brown University, Providence, RI 02912, USA*
† Electronic supplementary information (ESI) available. See DOI: https://doi.org/10.1039/d5en00376h

1. Introduction

Nanoscale particles exist naturally and through anthropogenic activities, including through intentional application[1–8] and unintentional release.[9,10] Their unique physiochemical material properties have raised concerns regarding their impact on human health and the environment. Nanoparticle mobility of is a key factor that determines their bioavailability and subsequent risk of exposure.[11,12] Deposition and aggregation are fundamental behaviors influencing particle mobility in addition to material reactivity.[13,14] Colloid aggregation has been classically modelled as a force balance, based on van der Waals attraction and electrostatic repulsion in the presence of various electrolytes (*i.e.*, Derjaguin–Landau–Verwey–Overbeek, DLVO, theory).[13,15,16] However, in real-world systems, the presence of organic molecules such as natural organic matter (NOM), alginate, and proteins can significantly alter aggregation behavior, leading to deviations from classic DLVO predictions.[17–21] For such interactions, non-DLVO forces such as depletion attraction, steric repulsion, bridging, and patch-charge attraction can significantly influence particle stability.

Among various environmental coatings, glycolipids have been understudied despite being ubiquitously produced by a number of biological systems.[22] Specifically, rhamnolipids (RL) have gained interest due to their amphiphilic properties and relatively low critical micelle concentration (CMC).[23–28] RLs are produced by *Pseudomonas aeruginosa*, among other bacteria, and play a key role(s) in biofilm maturation stages.[29–31] Field studies have confirmed their presence in undisturbed, metal-contaminated and hydrocarbon-contaminated soils.[32,33] A contaminated groundwater site at a former refinery in Michigan reported RL concentrations of 50 ppm, while levels as high as 1000 ppm have been observed under low nitrogen conditions.[34,35] In addition to naturally occurring, RLs have also been applied for enhanced bioremediation and oil recovery as they can effectively mobilize hydrophobic molecules.[36–38] Further, as a natural surfactant, there is potential for their use in eco-friendly pharmaceuticals, cosmetics, and detergent formulations.[25,39]

Two predominant species of RL observed are mono- and di-rhamnolipid(s) with one (mono) or two (di) rhamnose residues, respectively, forming a polar head group(s), which are linked through a beta-glycosylic bond to two 3-hydroxy fatty acids (depicted in Fig. S1†).[40] These anionic, amphiphilic molecules exhibit a high propensity to interact with both organic and inorganic molecules due to their surface-active nature and very low Gibbs free energy of adsorption.[26,27] Due to their ubiquitous environmental presence along with surface-altering interfacial properties, a quantitative understanding of RL–nanoparticle interactions is essential for developing more accurate fate and transport models.

In this study, we elucidate the role of monorhamnolipid (monoRL) and dirhamnolipid (diRL) on the aggregation dynamics of engineered IONPs as a function of particle surface charge and solution chemistry. Iron oxide nanoparticles (IONPs) were surface-modified with a cationic surfactant (cetyltrimethylammonium bromide, CTAB) and an anionic surfactant (sodium dodecylbenzene sulfonate, SDBS) to form monodisperse suspensions in water.[41] 8 nm monodispersed iron oxide nanoparticles were chosen as they are identical in shape and size (thus allow for direct comparison and straightforward modeling), while being superparamagnetic, thus allowing for low energy separations if needed. To the best of our knowledge, this is the first systematic study which quantifies the impact of RL on the aggregation dynamics, including kinetics, of surface engineered nanoparticles.

2. Materials and methods

2.1. Materials

Iron(III) oxide (hydrated, catalyst grade, 30–50 mesh), 1-octadecene (technical grade, 90%), oleic acid (technical grade, 90%), hexadecyltrimethylammonium bromide (CTAB, ≥98% solids), sodium dodecylbenzene sulfonate (SDBS, technical grade), sodium chloride (ACS reagent, ≥99.0%), magnesium chloride (ACS reagent, ≥99.0%), and sodium sulfate (ACS reagent, ≥99.0%, anhydrous, granular) were purchased from Sigma Aldrich and used without further purification. Monorhamnolipid and dirhamnolipid (95% purity) were purchased from AGAE Technologies and quantified using total organic carbon analyzer.

2.2. Synthesis of surface modified IONPs

2.2.1. Synthesis of IONPs. IONPs were synthesized using the method reported by Li *et al.*[42] 0.178 g FeO(OH) finely powdered, 2.26 g oleic acid and 5.0 g 1-octadecene were stirred in a three-necked flask equipped with a heating mantle and temperature controller and heated to 120 °C for 1 h to remove excess water and then to 320 °C at constant argon flow conditions. After the reaction at high temperature, the resulting brown-black colloid was let to cool off and then purified by washing it 4–5 times with acetone and methanol by centrifugation at 8000 rpm for 10 min. This was done to remove unreacted iron salts, 1-octadecene, and excess oleic acid. After the final wash, the nanoparticles were stored in dark conditions in hexane.

2.2.2. Phase transfer of IONPs. The IONPs in hexane are hydrophobic in nature. To make the IONPs dispersible in aqueous phase a bilayer strategy was used.[41] The hydrophobic NPs were transferred to water by combining 1 mL of IONP (5 g L^{-1}) with different amount of CTAB and SDBS surfactant in Milli Q water (Millipore, 18.2 Ω) in a glass vial to a total volume of 10 mL. The mixture of organic and aqueous phase was then subjected to a probe sonicator (UP 50H, Dr. Hielscher, GMBH) for 2–5 min at various amplitudes (60–90%) and full cycle. The resulting cloudy suspension of surfactant-IONPs was stirred for a day to evaporate residual hexane. The aqueous phase was collected and washed with

Milli Q water 2–3 times to separate out the unstable particles. Residual surfactants were removed by Amicon stir cell membrane filtration (100 kDa MWCO), by washing with MilliQ water 5–6 times or until no more surfactant was visibly present in the filtrate. The residue was then redispersed in MilliQ water and filtered using a syringe filter (pore size of 0.45 μm, Millipore).

2.3. Characterization of IONPs

2.3.1. Transmission electron microscope (TEM). IONP core size was characterized by transmission electron microscopy (TEM, FEI Tecnai G2 Spirit) operated at 120 kV. TEM samples were prepared by placing a drop (10 μL) of the 100 times diluted NP suspension on a carbon coated copper grids (Electron Microscopy Sciences) and allowed to dry at room temperature (22 ± 0.5 °C). The average diameter (with size distribution) was obtained by counting more than 500 randomly chosen NPs from the TEM micrographs using ImageJ software (National Institutes of Health).

2.3.2. Inductively coupled plasma optical emission spectroscopy (ICP-OES). To determine the concentration of IONPs (as Fe) and the yield of IONPs transferred from hexane to water phase, IONPs were digested in nitric acid (trace metal grade, 10%) and analyzed using inductively coupled plasma optical emission spectroscopy (ICP-OES, Perkin Elmer ELAN DRC).

2.3.3. Dynamic light scattering (DLS). The hydrodynamic diameter and zeta potential (ζ) of IONPs in water were measured by dynamic light scattering (Nanobrook Omni, Brookhaven Instruments). Triplicate samples were prepared and measured for the size and ζ analysis. The average value and the standard deviation of size and ζ were calculated from at least 10 measurements. Given that the nanoparticles are spherical, hydrophilic, and were characterized under conditions of ionic strength exceeding 10 mM, the Smoluchowski approximation was deemed appropriate and employed to convert electrophoretic mobility (measured *via* DLS) into zeta potential.[43,44]

2.3.4. Total organic carbon (TOC). Grafting density of the surfactants (CTAB, SDBS) on the nanoparticle surface was quantified using total organic carbon analyzer (TOC-L, Shimadzu Scientific Instrument, Inc., MD; 680 °C). Surface modified nanoparticles were separated using an ultracentrifuge (Thermo Scientific Sorvall WX) at 45 000 rpm for 2 h. TOC of the samples was measured before and after separating the NPs.

2.4. Tensiometric analysis of RLs

The RLs (monoRL, diRL) micellar concentration was quantified using Wilhelmy plate, force tensiometer (Attention 700, Biolin Scientific). Surface tension of RLs at concentration ranges of 0–100 mg L^{-1} of organic carbon (OC, measured using TOC) at pH 7.2 were measured in triplicate. After each measurement, the plate was subjected to a cleaning process involving sequential flushing with ethanol and water, followed by exposure to high temperature *via* Bunsen burner until the Wilhelmy plate achieved a red glow. The initial point at which the surface tension values starts to plateau with respect to RL concentration is the critical micelle concentration (CMC) of the respective RLs (mono or di).[45]

2.5. Batch adsorption experiments

Adsorption of monoRL and diRL on IONP (10 ppm as Fe) was measured at pH 7.2 at 22 °C. After 24 h of equilibration time in an orbital shaker unadsorbed RL was separated using ultracentrifuge (Sorvall WX Ultra 80, Thermo Scientific) at 45 000 rpm for 2 h. The supernatant was measured using TOC-L and LCMS (6470B Triple Quadrupole, Agilent Technology) with a C18 reverse phase column. For the LCMS, the organic phase used was acetonitrile (Optima™ LCMS Grade, Fisher Chemicals) and the aqueous phase used was 0.1% formic acid in water (Optima™ LC/MS Grade) with 0.4 mL min^{-1} of flow rate and injection volume of 50 μL. Electrospray ionization was performed in negative mode with 135 V as fragmentor voltage, 5 V as cell accelerator voltage, 300 °C AND 250 °C as gas and sheath gas temperatures, 5 L min^{-1} and 11 L min^{-1} as gas flow and sheath gas flows, 45 psi as the nebulizer pressure, and 3500 V and 500 V as the capillary and nozzle voltages respectively. Mass to charge ratios (m/z) of 503 and 649 corresponded to monoRL and diRL, respectively.[46] Calibration curves were prepared using different concentrations of mono/diRL at retention times of 7.8 and 6.7 minutes. The adsorption density *vs.* the equilibrium concentration of rhamnolipids was fit using Langmuir, Freundlich, Redlich–Peterson, and Sips isotherms.[47] Analytical expression of the models can be found in Table S2 in ESI.† The fitting parameters were obtained using Solver in Excel where the sums of squares difference of experimental adsorption density and theoretical adsorption density were minimized.

2.6. Aggregation kinetic

The aggregation kinetics of IONPs in the presence of RLs with and without salt addition was studied using a DLS equipped with a 40 mW diode laser with nominal wavelength of 640 nm (Nanobrook Omni, Brookhaven Instruments), operating in backscattering mode at a scattering angle of 173°. Before each aggregation measurement, a predetermined volume of NP stock solution and ultrapure water were added into a vial and pH was adjusted to 7.2 ± 0.2. Predetermined amounts of salt solution and/or RLs were added to the vial to obtain a total volume of 1 mL and the concentration of IONPs 10 mg L^{-1} (as Fe). All experiments were conducted at 22 °C. Samples were transferred into the DLS measurement chamber after vortex mixing for 2–5 s. Data points were measured every 15 s and recorded continuously until 2 times the initial hydrodynamic diameter (a_h) was achieved. The initial aggregation rate constant (k) of IONPs was determined from a linear least square regression analysis of change in a_h with time (t) as shown in eqn (1).

$$k \propto \frac{1}{N_0}\left(\frac{\mathrm{d}a_h(t)}{\mathrm{d}t}\right)_{t\to 0} \quad (1)$$

Here, N_0 is the initial particle concentration. In this study, the attachment efficiency (α), known as the inverse stability ratio, was calculated by normalizing the measured k by the diffusion-limited aggregation rate constant, k_{fast}. The attachment efficiency ranges from 0 to 1, representing the probability of an irreversible attachment resulting from the collision of two particles. The attachment efficiency (α) of the IONPs in the presence of monovalent and divalent electrolytes was calculated using eqn (2).[18,48,49]

$$\alpha = \frac{k}{k_{fast}} = \frac{\frac{1}{N_0}\left(\frac{\mathrm{d}a_h(t)}{\mathrm{d}t}\right)_{t\to 0}}{\frac{1}{N_{0,fast}}\left(\frac{\mathrm{d}a_h(t)}{\mathrm{d}t}\right)_{t\to 0,fast}} \quad (2)$$

3. Results and discussion

3.1. Characterization of IONPs

Synthesized IONPs were monodispersed and uniform in shape, with a core diameter of 8 nm, as shown in Fig. S2 (ESI†). Upon the addition of surface coatings, the average number mean hydrodynamic diameter of the CTAB-IONPs and SDBS-IONPs are 14.4 ± 3.08 and 15.7 ± 2.8 nm, respectively. Optimized aqueous transfer concentrations (and corresponding procedure) of the ligands are presented in Table S1 (ESI†). For materials studied here, ligand densities of CTAB and SDBS on IONP are 718 ± 72 and 830 ± 100 molecules per IONP, respectively. Calculations for quantifying grafting density are included in ESI† (Fig. S14). Zeta potential (ζ-potential), as a function of pH, is shown in Fig. S3.† Both IONPs suspensions are stable at circumneutral pH for months in pure water.

3.2. Aggregation of IONPs without RLs

Electric double layer (EDL) repulsion is strongly dependent on particle surface charge. Here, IONP aggregation was studied at pH 7.2, at which measured ζ-potential values for CTAB- and SDBS-IONPs were 30.2 and −27.8 mV, respectively (Fig. S3†). To compare the impact of RLs on IONP aggregation, establishing baseline stability regime(s) without RLs is critical as a control for comparison(s). Fig. 1(a) shows the attachment efficiency of IONPs as a function of monovalent (NaCl) and divalent salts ($MgCl_2$ and Na_2SO_4), without the presence of RLs. For SDBS-IONPs, we observed a typical aggregation profile which can described *via* classical DLVO theory.[50,51] By increasing the ionic strength of the solution, the repulsive energy barrier between the IONPs was gradually minimized such that particles undergo reaction limited aggregation ($\alpha < 1$). Upon further increase in ionic strength, a diffusion limited aggregation regime was observed (alpha ≅ 1), and the aggregation rate did not change with additional electrolyte (Fig. 1 and S5†). The concentration of electrolyte at which the two aggregation regimes coincide, termed the critical coagulation concentration (CCC), for SDBS-IONP was 700 mM and 15 mM in presence of Na^+ and Mg^{2+} electrolytes, respectively. The CCC value of SDBS-IONPs in Mg^{2+} electrolyte was smaller than CCC obtained in Na^+ by ~47×, which is in good agreement with the Schulze–Hardy rule (*i.e.*, the CCC is inversely proportional to the valency of the counter ions raised to its inverse sixth power ($1:2^{-6}$)).[50–52]

For CTAB-IONP, we did not observe a diffusion limited aggregation regime as evident in Fig. 1(a) and S6,† although the ζ-potential decreased from 30.2 mV to less than 5 mV in the presence of high NaCl concentrations (Fig. 1(b)). This indicates that neither Cl^- or SO_4^{2-} anions, at concentration ranges studied, were sufficient to completely compress the electric double layer (EDL) of CTAB-IONP (Fig. 1(a)) and/or steric hindrance from the methyl group of the tertiary amine in the CTAB prevented homoaggregation (Fig. S14(a)†). Previously, Li *et al.* noted the CCC of CTAB (12-carbon) to be 555 mM NaCl, but due to effect of chain length of CTAB (16-carbon) used in this study, it is likely to have a higher CCC than that of CTAB (12-carbon chain)-IONP.

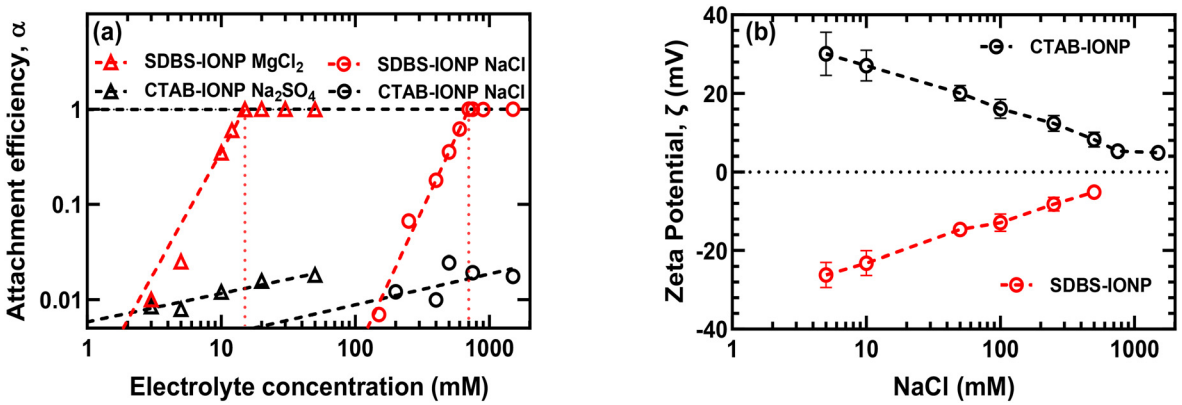

Fig. 1 (a) Attachment efficiency (α) of 10 mg L^{-1} (as Fe) CTAB-IONP and SDBS-IONP as a function of monovalent (NaCl) and divalent ($MgCl_2$, Na_2SO_4) salt in log–log scale and (b) zeta potential (ζ) of 10 mg L^{-1} (as Fe) CTAB-IONP and SDBS-IONP as a function of NaCl concentration at pH 7.2.

While CCC is often interpreted based on ion valence, recent studies suggest that surface charge density provides a more mechanistic understanding of coagulation behavior.[53–55] However, in this study, the nanoparticles are sterically stabilized by surface-active agents (CTAB and SDBS), where zeta potential—and consequently surface charge density—may not completely underpin colloidal stability. Thus, while the concept of surface charge density is useful for highly electrostatically stabilized systems, it may not be as applicable to particles systems with additional stabilizing factors, such as steric interactions, *etc.*

3.3. Effect of RLs on IONP behavior

Based on amphiphilic structure and low CMC values (10.1 and 20.9 mg of OC L^{-1} for diRL and monoRL, respectively) (Fig. S4†), we hypothesize that RLs are likely to affect the surface activity of nanoparticles suspended in water. To quantify this effect, we measured IONPs aggregation in the presence of monoRL and diRL at pH 7.2. SDBS-IONP aggregation was unaffected upon addition of RLs over the range of concentrations studied as shown in Fig. S6,† due to both species being anionic. The ζ-potential of monoRL and diRL micellar solution was −28.89 ± 2.3 mV and −35.62 ± 5.67 mV, respectively. Interestingly, RLs, especially at higher concentration, were adsorbed on SDBS-IONPs (Fig. 2(b)) which is likely due to hydrogen bonding between the sulfonate group and the proton in the rhamnose moiety of RL.[56–58] Experimental data of RL adsorption on CTAB- and SDBS-IONP is shown in Fig. 2, with model parameters and best fitting isotherm models summarized in Table S2.† MonoRL and diRL adsorption on CTAB-IONP exhibited best fit(s) when considering a multilayer adsorption model (Sips) with R^2 = 0.99. Adsorption densities increased in a near linear fashion and then stabilized once the equilibrium concentration was greater than the CMC (monoRL = 20.9 and diRL = 10.1 mg as organic carbon, OC L^{-1}). This observation was attributed to the formation of RL micelles in the aqueous solution rather than adsorbing on the IONP surface itself.[59] MonoRL and diRL adsorb to a lesser extent on anionic SDBS-IONP at lower concentrations; however, at concentrations higher than the CMC, micelles adsorb onto the anionic IONP surface. Both SDBS-IONP isotherms (monoRL and diRL) were best fit with a Freundlich model (R^2 = 0.91 and 0.996, respectively, Table S2†).

As a function of RL concentration(s), three distinct stability regimes are observed for CTAB-IONP in the presence of monoRL and diRL. The first regime is observed for RL concentrations below 10 and 5 mg L^{-1} OC for monoRL and diRL, respectively, whereby the nanoparticles are stable, and negligible aggregation is observed, as shown in Fig. 3. At these RL concentration ranges, the ζ-potential of the systems is above +20 mV, which suggests particle stability is primarily due to electrostatic repulsion of CTAB-IONPs (Fig. 3b). As the RL concentration is further increased, we observed an intermediate regime where CTAB-IONPs lose stability and aggregate. The isoelectric points of the CTAB-IONPs were reached at concentrations of 12.5 and 20 mg L^{-1} OC for diRL and monoRL, respectively. For these cases, the double rhamnose moiety in diRL likely provides additional hydrophilic interactions compared to monoRL. CTAB-IONPs are observed to re-stabilize after 20 and 30 mg L^{-1} OC of diRL and monoRL, respectively. Here the ζ-potential was −15 mV for both, becoming more negative with further addition of RLs. A similar surface charge reversal has been observed previously for NPs in presence of humic acid, alginate, and cytochrome proteins.[19,60]

To better understand aggregation mechanism(s) and resulting surface chemistry of the subsequent aggregated systems, CTAB-IONP partitioning into a (hydrophobic) hexane phase (from water) was explored as part of the previous experimental matrix (Fig. S9†). For the intermediate

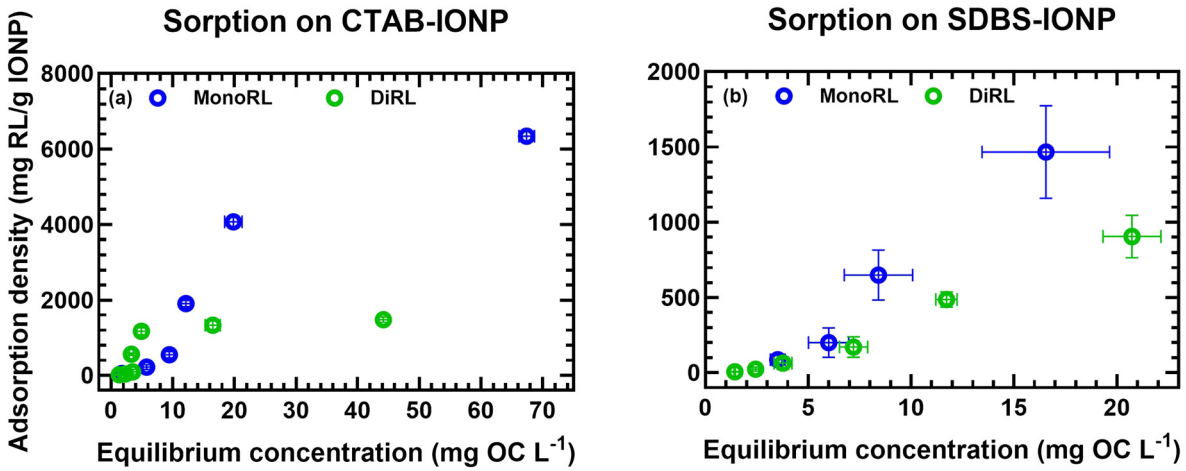

Fig. 2 Experimental data of adsorption density as a function of equilibrium concentration of monoRL and diRL on (a) CTAB-IONP and (b) SDBS-IONP at T = 22 °C and pH = 7.2. Concentration of IONP used in the study is 10 mg L^{-1} (as Fe). Details of parameters of all studied isotherms can be found in in Table S2 in ESI.†

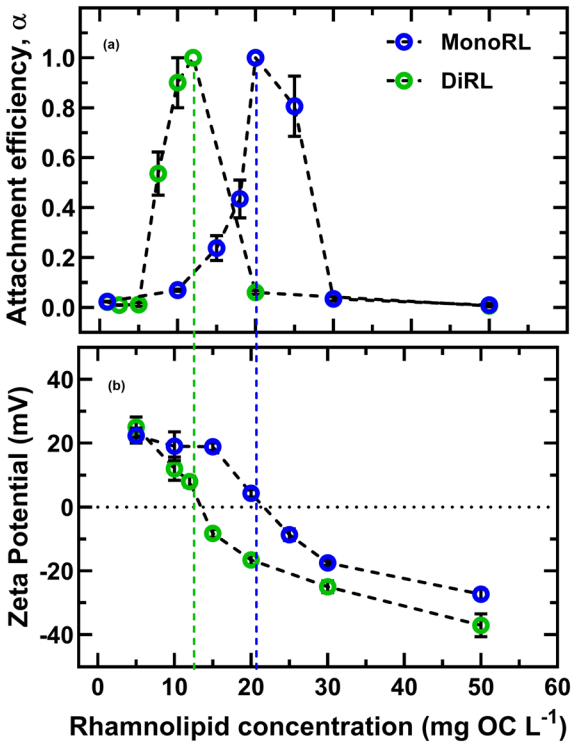

Fig. 3 (a) Attachment efficiency of 10 mg L^{-1} of CTAB-IONP as a function of rhamnolipid concentrations and (b) zeta potential of CTAB-IONP at corresponding concentration of RLs at pH 7.2.

concentration range (with effectively near neutral ζ-potential), CTAB-IONP partitioning into hexane was observed to be enhanced (Fig. S9(c) and (d)†). This is due to the IONPs becoming effectively hydrophobic upon attachment of diRL in a head-to-tail orientation, whereby the hydrophobic tail points outwards. With additional RL, IONPs become hydrophilic again and favorably remain in the aqueous phase (Fig. S9(e)†). A proposed model of this dynamic is illustrated in Fig. 4. We assume that micelles are not adsorbed on the IONP surface as the average hydrodynamic diameter of CTAB-IONP before and after bilayer formation was 14.4 nm and 19.62 nm, respectively, whereas the size of RL micelles is reported in the range of 40–90 nm.[61,62] The adsorption density *vs.* initial RL concentration (Fig. S8†) was used to calculate the number of RL molecules per IONP in Table S3.† We estimated that *ca.* 830 and 1325 molecules of diRL and monoRL adsorb per IONP, respectively, to form a monolayer which equals 1.15 ± 0.08 and 1.85 ± 0.24 molecule per CTAB ligand. The number of monoRL molecules attached on CTAB-IONP was significantly more than that of DiRL due to steric effects from the additional rhamnose group. A bilayer was formed upon the addition of 0.82 ± 0.29 and 1.08 ± 0.41 molecules of diRL and monoRL respectively, per monolayer of RL.

3.4. Effects of ionic strength and surface associated RL(s) on anionic IONP aggregation behavior

While RL did not induce significant SDBS-IONP aggregation (Fig. S7†), its adsorption alters surface activity (Fig. 2(b)). Here, we hypothesize that adsorbed RL increases the CCC of the SDBS-IONP due to both increased electrostatic and steric

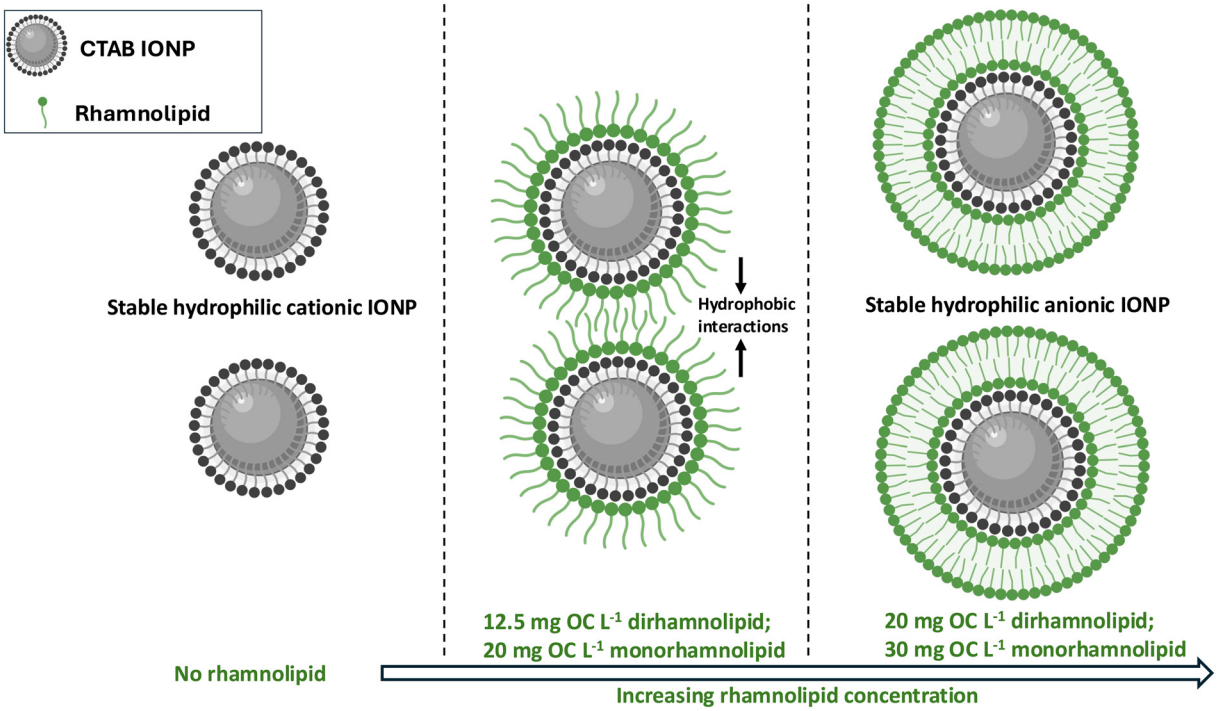

Fig. 4 Proposed model for aggregation of CTAB-IONP where the blue sphere is the core IONP and black and green curved lines are CTAB ligand and rhamnolipids, respectively.

Table 1 Summarized critical coagulation concentration (CCC) of anionic IONP (SDBS-IONP) in presence of monovalent NaCl and divalent $MgCl_2$ salts

Amount of rhamnolipid added to SDBS-IONP	NaCl CCC (mM)	$MgCl_2$ CCC (mM)	n
No RL	700	15	5.56
1 mg OC L^{-1} monoRL	700	15 (α = 0.63)	5.56
5 mg OC L^{-1} monoRL	800	15 (α = 0.68)	5.73
10 mg OC L^{-1} monoRL	900 (α = 0.82)	20 (α = 0.65)	5.49
1 mg OC L^{-1} diRL	800	22.5 (α = 0.7)	5.15
5 mg OC L^{-1} diRL	900	25 (α = 0.65)	5.16
10 mg OC L^{-1} diRL	1500 (α = 0.75)	30 (α = 0.57)	5.64

repulsive forces. The attachment efficiency *versus* electrolyte concentration of SDBS-IONP in presence of RLs followed typical DLVO behavior with well-defined reaction-limited and diffusion-limited regimes (Fig. S5†). The CCC values for varied RL concentrations in presence of NaCl and $MgCl_2$ are presented in Table 1 and summarized in Fig. 5 (derived from Fig. S10† analysis). SDBS-IONP CCC in the absence of RL was 700 mM NaCl (Fig. 1(a)), which increased to 900 mM and 1500 mM in presence of 10 mg OC L^{-1} of monoRL and diRL, respectively. The α value in presence of 10 mg OC L^{-1} for both RLs (Fig. S9†) was less than 1 in the diffusion limited aggregation regime, which is attributed to increased steric repulsion.[19]

Attachment efficiency of SDBS-IONP as a function of divalent cations ($MgCl_2$) is also shown in Fig. S10(c) and (d)† with a CCC 15 mM. The valency of the counterion strongly influences the electric double layer repulsion barrier[63,64] as described by:[65]

$$\mathrm{CCC} \propto z^{-n},\ n = 6$$

Here, z is the valency of the counterion; n values are tabulated in Table 1. Similar to monoRL, upon the addition of 1, 5, 10 mg OC L^{-1} of diRL, CCC increased to 22.5, 25, 30 mM. Thus, diRL also provides enhanced stability to the SDBS-IONP in high(er) ionic strength conditions. In addition to classic DLVO forces governing the aggregation of SDBS-IONP, extended-DLVO forces, likely influence behavior at higher RL concentrations (Fig. S10†).

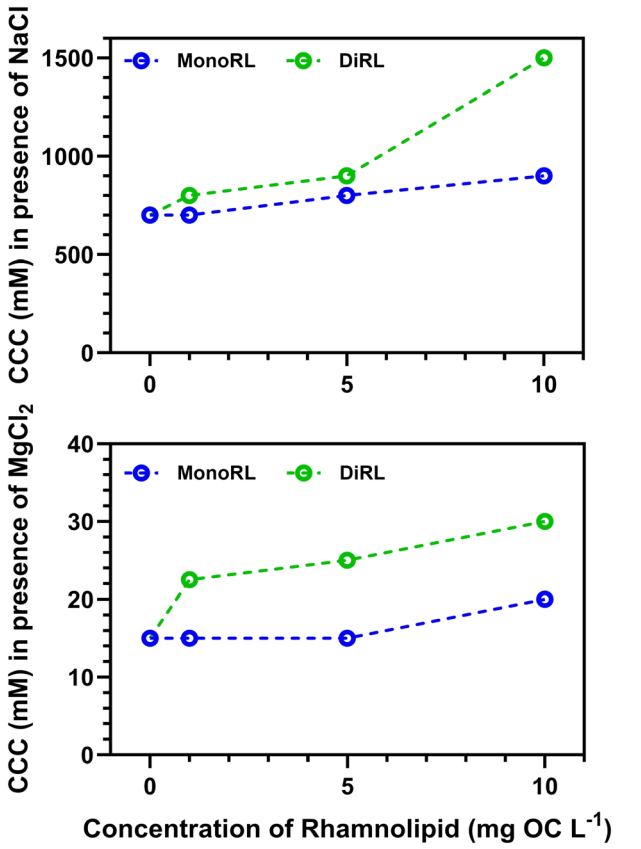

Fig. 5 Critical coagulation concentrations (mM) of SDBS-IONP with increasing concentration of monoRL and diRL in presence of (a) monovalent NaCl and (b) divalent $MgCl_2$. CCC values are derived from stability analyses detailed in Fig. S10 (ESI†).

3.5. Effects of ionic strength and surface associated RL(s) on cationic IONP aggregation behavior

CTAB coatings significantly enhance NP stability (Fig. 1(a) and S6†). This stability was attributed to steric hindrance arising from the three methyl groups surrounding the amine headgroup. As shown in Fig. 3(a), RLs can lead to dynamic IONP aggregation (also depicted in Fig. 4). To elucidate the effect of ionic strength on the aggregation of RL coated CTAB IONPs, stability behavior was divided into 3 regimes as shown in Fig. 6(a) and 7(a) for monoRL and diRL, respectively. Three points (A, B, and C) were selected from each distinct aggregation regime to further understand the role of ionic strength and type within these regimes, considering monovalent and divalent anions as Cl^- and SO_4^{2-}.

For point A (within regime 1), CTAB-IONPs are only partially covered by monoRL/diRL according to the proposed model in Fig. 4 and ligand coating density analysis. Upon the addition of NaCl and Na_2SO_4, shown in Fig. 6(b) and (c), a reaction limited regime is reached relatively fast as IONPs readily aggregate. The CTAB-IONP-monoRL (10 mg L^{-1}, light blue circle Fig. 6(a) and (b)) begin to aggregate upon addition of 20 mM of NaCl or 4 mM Na_2SO_4. For these, neither the presence of electrolytes (even at high concentrations), or 10 mg L^{-1} of monoRL by itself induced CTAB-IONP aggregation.[66] The maximum α value in this regime was 0.7 and 0.8 for NaCl and Na_2SO_4, respectively. The addition of salt also reduced the ζ-potential of the particles, thus promoting the screening of the net positive charge by weakening the electrostatic repulsion of the CTAB-IONP (Fig. S11†). At higher salt concentrations, 1000 mM and 50 mM of NaCl and Na_2SO_4, respectively, IONPs were observed to stabilize, which was not due to electrostatic repulsion as the zeta potential value at 1000 mM of NaCl (Fig. S11†) is 0.25 ± 0.98 mV. Fig. S12† shows that at higher salt concentration almost 20%

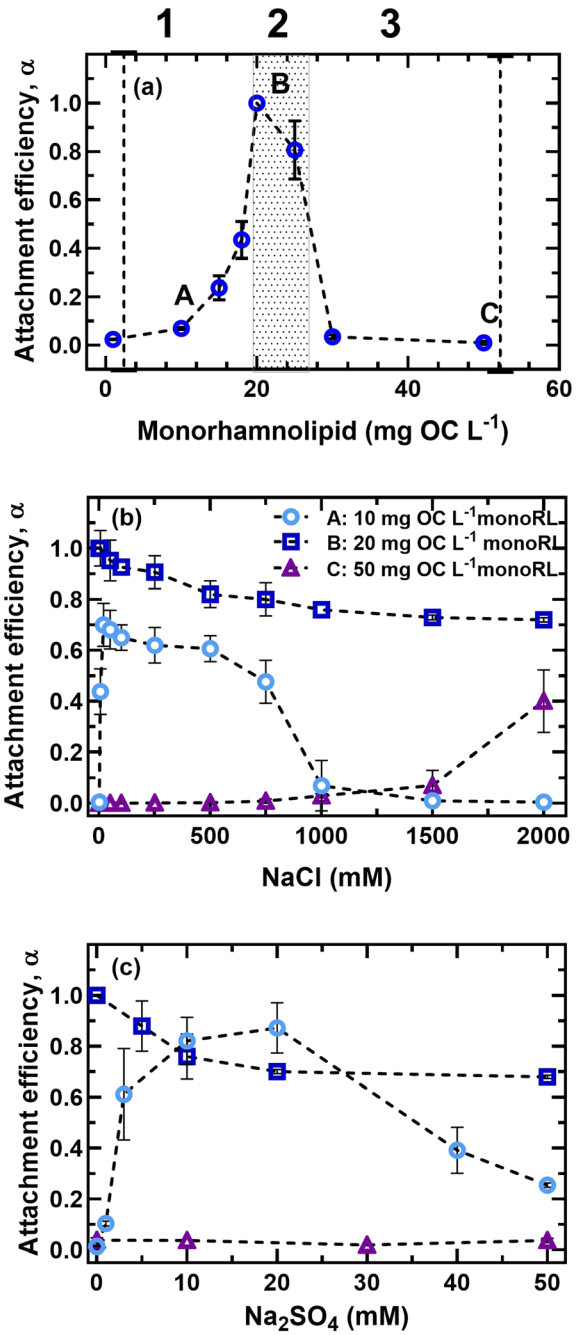

Fig. 6 Attachment efficiency of CTAB-IONP as a function of (a) monoRL concentration at pH 7.2 divided into three distinct regions 1, 2 and 3 based on three different aggregation regimes, (b) attachment efficiency at 3 random points (A, B, and C from Fig. 6(a) where 10, 20 and 50 mg L^{-1} OC of monoRL are A, B, and C respectively) as a function of NaCl, and (c) Na_2SO_4 concentration.

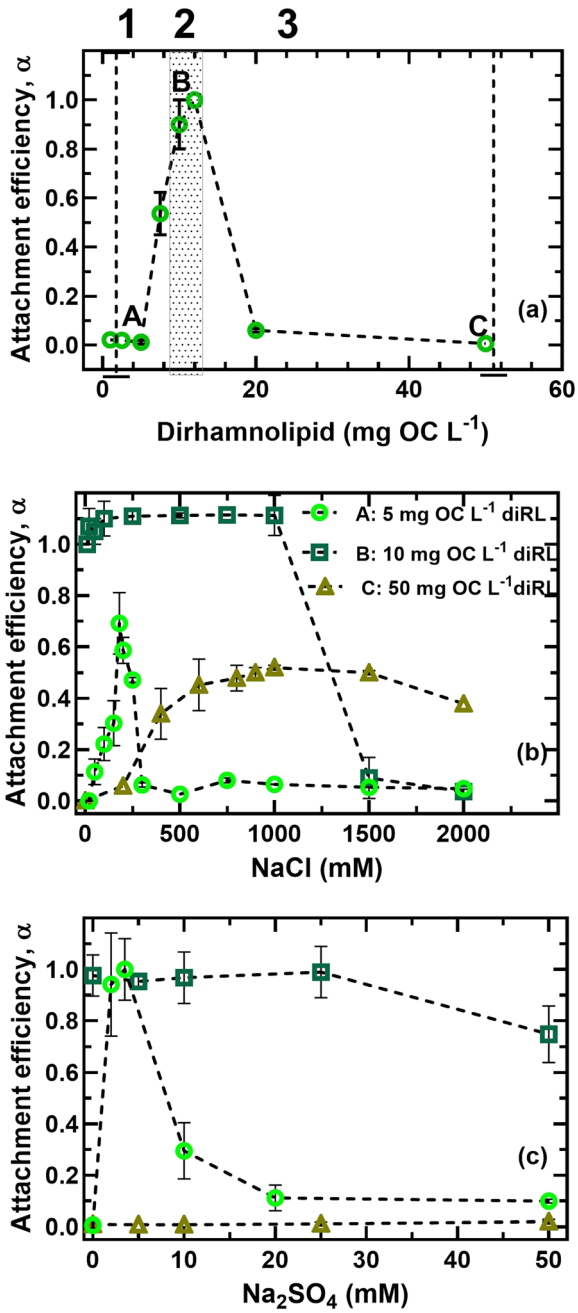

Fig. 7 Attachment efficiency of CTAB-IONP as a function of (a) diRL concentration at pH 7.2 divided into three distinct regions 1, 2, and 3 based on aggregation regimes. (b) Attachment efficiency at 3 random points (A, B, C from Fig. 7(a), where 5 mg L^{-1}, 10 mg L^{-1} and 50 mg L^{-1} of diRL are A, B and C respectively) as a function of NaCl, and (c) Na_2SO_4 concentration.

monoRL was actually released from the surface of CTAB-IONP compared to no or low salt addition. Such desorption of monoRL from surface resulted in surface 'patching' and charge alteration.[19] Similar aggregation–disaggregation behavior of IONPs was also seen in point A of regime 1 in presence of diRL and salt (Fig. 7(b) and (c)), although the aggregation range was narrower compared to monoRL, which could be due to diRL being relatively more polar with a larger MW. Disaggregation (*i.e.*, restabilization) occurred upon the addition of 300 and 20 mM of NaCl and Na_2SO_4 respectively. TEM micrographs of aggregation(–disaggregation) dynamics are shown in Fig. S13,† which were collected at equilibrium (>one hour reaction).

In Fig. 6(a) and 7(a), in regime 2 and at/near point B, mono/diRL forms a monolayer around the CTAB-IONP, as discussed earlier, and hydrophobic interactions dominate the

system. With addition of both NaCl and Na_2SO_4, there was negligible change in the attachment efficiency compared to regime 1. The addition of the salt slightly reduced the attachment efficiency as shown in Fig. 6(b) and (c). In case of diRL, similar behavior was observed – except at 1500 mM of NaCl whereby enhancement in stabilization occurred, which could be due to change(s) in micelle-like structure of diRL (and/or release of DiRL) and/or screening of patch charge attraction at higher salt concentrations.

In regime 3, without salt addition, CTAB-IONP in presence of mono/diRL was completely stable with a charge reversal observed (Fig. 3(b)). According to our proposed model (Fig. 4), in this regime, a RL bilayer forms around the CTAB-IONP. In the presence of NaCl, diRL bilayer stabilized CTAB-IONPs showed a DLVO type aggregation profile with some (likely) steric hindrance (Fig. 7(b)). The CCC of RL bilayered CTAB-IONP was 750 and 2000 mM NaCl in presence of diRL and monoRL, respectively. No aggregation was observed in presence of divalent salts over the concentration ranges studied. Such high observed CCC values, due to RL bilayer coatings, present a potential 'green' stabilizing NP strategy for a variety of particle-based environmental applications which require high particle stability.

While this study evaluates the effect of Na^+, Ca^{2+}, Cl^- and SO_4^{2-} on IONP aggregation in the presence of rhamnolipids, it is important to note that natural aquatic systems typically contain a mixture of ionic species. Previous studies have shown that mixed ion compositions, particularly the coexistence of monovalent and divalent cations, can influence nanoparticle stability in non-additive ways.[67,68] Future work should explore such combined effects.

4. Conclusion

To date, the majority of studies on nanoparticle (NP) transport in environmental systems have focused on the effects of ionic strength and macromolecules such as natural organic matter, alginate, and proteins.[18,49,64] Few of these studies focused specifically on the potential role of biolipids. Here, we quantitatively demonstrate that rhamnolipids (RLs), produced by bacteria such as *Pseudomonas aeruginosa*, can significantly influence the aggregation behavior of iron oxide nanoparticles (IONPs) across a wide range of conditions, depending on the surface (chemistry) of the IONPs and aqueous chemistries.

Both RLs studied were found to adsorb onto both cationic and anionic IONPs, leading to highly stable cationic IONPs that can switch between aggregated and disaggregated phases based on the degree and orientation of RL sorption. Additionally, we show a synergistic effect of RL(s) and electrolyte(s) on the aggregation kinetics of both cationic and anionic IONPs. For anionic IONPs, increasing the ratio of RL to IONP resulted in higher CCC values (*i.e.*, increased stability). We propose that RLs form monolayer(s) and then bilayer(s) on cationic IONPs, leading to aggregation at intermediate RL to IONP ratios and then re-stabilization at higher RL to IONP ratios. At lower RL ratios, we observed aggregation–disaggregation behavior with increasing salt concentration, due to the release of RLs from CTAB-coated IONPs. At higher concentrations, whereby RLs form a bilayer (around CTAB-coated IONPs), we observe highly stable particles (*i.e.*, high CCC values).

Taken together, this study clearly and quantitatively demonstrates the importance of surface charge, RL type and ligand grafting density, and associated dynamics on particle behavior under varied ionic strength conditions. Building on these findings, the complex role of glycolipids on fundamental NP fate and transport in biotic environments should be further explored, as their effects are likely to be significant.

Data availability

Data can be found in the manuscript, ESI,† and at **https://openscholarship.wustl.edu**.

Author contributions

Anushree Ghosh: conceptualization, methodology, investigation, writing – original draft, visualization and analysis; Neha Sharma: synthesis, data curation and writing – review and editing; Junseok Lee: validation and analysis; Wenlu Li: synthesis and resources; Ji-Won Son: visualization and writing – review and editing; Changwoo Kim: methodology and analysis; Natalie L. Cápiro: conceptualization, supervision and funding acquisition; Kurt Pennell: conceptualization, resources, supervision and funding acquisition; Kimberly M. Parker: data curation, resources and methodology; John D. Fortner: conceptualization, project administration, supervision, writing – review and editing and funding acquisition.

Conflicts of interest

There are no conflicts to declare.

Acknowledgements

TEM and ICP-OES were performed in Nano Research Facility (NRF) in Washington University in St. Louis. LCMS analysis was performed at the Parker Lab in Washington University in St. Louis. ICP-MS and TOC-L analyzer tests were performed at Yale Analytical and Stable Isotope Center (YASIC) at Yale University with the help of Jonas Karosas. Surface tension measurements were conducted at Brown University with the help of Dr. Shuchi Liao. This work was supported by the U.S. Department of Agriculture, NIFA (2018-67021-28319) and the US National Science Foundation (award number CBET-170536).

References

1 Y. Zou, X. Wang, A. Khan, P. Wang, Y. Liu, A. Alsaedi, T. Hayat and X. Wang, Environmental Remediation and

Application of Nanoscale Zero-Valent Iron and Its Composites for the Removal of Heavy Metal Ions: A Review, *Environ. Sci. Technol.*, 2016, **50**, 7290–7304.

2 W. Li, J. T. Mayo, D. N. Benoit, L. D. Troyer, Z. A. Lewicka, B. J. Lafferty, J. G. Catalano, S. S. Lee, V. L. Colvin and J. D. Fortner, Engineered superparamagnetic iron oxide nanoparticles for ultra-enhanced uranium separation and sensing, *J. Mater. Chem. A*, 2016, **4**, 15022–15029.

3 Y. Guo, F. Cao, X. Lei, L. Mang, S. Cheng and J. Song, Fluorescent copper nanoparticles: Recent advances in synthesis and applications for sensing metal ions, *Nanoscale*, 2016, **8**, 4852–4863.

4 C. Kim, S. S. Lee, B. J. Lafferty, D. E. Giammar and J. D. Fortner, Engineered superparamagnetic nanomaterials for arsenic(V) and chromium(VI) sorption and separation: quantifying the role of organic surface coatings, *Environ. Sci.: Nano*, 2018, **5**, 556–563.

5 M. Kah, Nanopesticides and Nanofertilizers: Emerging Contaminants or Opportunities for Risk Mitigation?, *Front. Chem.*, 2015, **3**, 64.

6 X. Han, K. Xu, O. Taratula and K. Farsad, Applications of nanoparticles in biomedical imaging, *Nanoscale*, 2019, **11**, 799–819.

7 Y. Jin, C. Jia, S. W. Huang, M. O'Donnell and X. Gao, Multifunctional nanoparticles as coupled contrast agents, *Nat. Commun.*, 2010, **1**, 1–8.

8 N. Scott and H. Chen, Nanoscale Science and Engineering for Agriculture and Food Systems, *Ind. Biotechnol.*, 2013, **9**, 17–18.

9 M. P. Tsang, E. Kikuchi-Uehara, G. W. Sonnemann, C. Aymonier and M. Hirao, Evaluating nanotechnology opportunities and risks through integration of life-cycle and risk assessment, *Nat. Nanotechnol.*, 2017, **12**, 734–739.

10 L. Sweet and B. Strohm, Nanotechnology—Life-Cycle Risk Management, *Hum. Ecol. Risk Assess.*, 2006, **12**, 528–551.

11 M. Simonin, B. P. Colman, S. M. Anderson, R. S. King, M. T. Ruis, A. Avellan, C. M. Bergemann, B. G. Perrotta, N. K. Geitner, M. Ho, B. de la Barrera, J. M. Unrine, G. V. Lowry, C. J. Richardson, M. R. Wiesner and E. S. Bernhardt, Engineered nanoparticles interact with nutrients to intensify eutrophication in a wetland ecosystem experiment, *Ecol. Appl.*, 2018, **28**, 1435–1449.

12 J. B. Glenn and S. J. Klaine, Abiotic and biotic factors that influence the bioavailability of gold nanoparticles to aquatic macrophytes, *Environ. Sci. Technol.*, 2013, **47**, 10223–10230.

13 E. M. Hotze, T. Phenrat and G. V. Lowry, Nanoparticle Aggregation: Challenges to Understanding Transport and Reactivity in the Environment, *J. Environ. Qual.*, 2010, **39**, 1909–1924.

14 A. M. Vindedahl, J. H. Strehlau, W. A. Arnold and R. L. Penn, Organic matter and iron oxide nanoparticles: aggregation, interactions, and reactivity, *Environ. Sci.: Nano*, 2016, **3**, 494–505.

15 K. M. Buettner, C. I. Rinciog and S. E. Mylon, Aggregation kinetics of cerium oxide nanoparticles in monovalent and divalent electrolytes, *Colloids Surf., A*, 2010, **366**, 74–79.

16 W. Li, D. Liu, J. Wu, C. Kim and J. D. Fortner, Aqueous aggregation and surface deposition processes of engineered superparamagnetic iron oxide nanoparticles for environmental applications, *Environ. Sci. Technol.*, 2014, **48**, 11892–11900.

17 K. L. Chen and M. Elimelech, Aggregation and deposition kinetics of fullerene (C60) nanoparticles, *Langmuir*, 2006, **22**, 10994–11001.

18 K. L. Chen and M. Elimelech, Influence of humic acid on the aggregation kinetics of fullerene (C60) nanoparticles in monovalent and divalent electrolyte solutions, *J. Colloid Interface Sci.*, 2007, **309**, 126–134.

19 A. Sheng, F. Liu, L. Shi and J. Liu, Aggregation Kinetics of Hematite Particles in the Presence of Outer Membrane Cytochrome OmcA of Shewanella oneidenesis MR-1, *Environ. Sci. Technol.*, 2016, **50**, 11016–11024.

20 M. Ren, H. Horn and F. H. Frimmel, Aggregation behavior of TiO2 nanoparticles in municipal effluent: Influence of ionic strengthen and organic compounds, *Water Res.*, 2017, **123**, 678–686.

21 J. Liu, C. Dai and Y. Hu, Aqueous aggregation behavior of citric acid coated magnetite nanoparticles: Effects of pH, cations, anions, and humic acid, *Environ. Res.*, 2018, **161**, 49–60.

22 M. Basnet, S. Ghoshal and N. Tufenkji, Rhamnolipid biosurfactant and soy protein act as effective stabilizers in the aggregation and transport of palladium-doped zerovalent iron nanoparticles in saturated porous media, *Environ. Sci. Technol.*, 2013, **47**, 13355–13364.

23 B. R. Boles, M. Thoendel and P. K. Singh, Rhamnolipids mediate detachment of Pseudomonas aeruginosa from biofilms, *Mol. Microbiol.*, 2005, **57**, 1210–1223.

24 S. S. Helvaci, S. Peker and G. Ozdemir, Effect of electrolytes on the surface behavior of rhamnolipids R1 and R2, *Colloids Surf., B*, 2004, **35**, 225–233.

25 K. K. S. Randhawa and P. K. S. M. Rahman, Rhamnolipid biosurfactants-past, present, and future scenario of global market, *Front. Microbiol.*, 2014, **5**, 454.

26 D. Mańko, A. Zdziennicka and B. Jańczuk, Thermodynamic properties of rhamnolipid micellization and adsorption, *Colloids Surf., B*, 2014, **119**, 22–29.

27 R. B. Lovaglio, F. J. dos Santos, M. Jafelicci and J. Contiero, Rhamnolipid emulsifying activity and emulsion stability: PH rules, *Colloids Surf., B*, 2011, **85**, 301–305.

28 S. S. Dashtbozorg, J. Kohl and L. K. Ju, Rhamnolipid adsorption in soil: Factors, unique features, and considerations for use as green antizoosporic agents, *J. Agric. Food Chem.*, 2016, **64**, 3330–3337.

29 S. Arino, R. Marchal and J.-P. Vandecasteele, Identification and production of a rhamnolipidic biosurfactant by a Pseudomonas species, *Appl. Microbiol. Biotechnol.*, 1996, **45**, 162–168.

30 E. Deziel, rhlA is required for the production of a novel biosurfactant promoting swarming motility in Pseudomonas aeruginosa: 3-(3-hydroxyalkanoyloxy)alkanoic acids (HAAs),

the precursors of rhamnolipids, *Microbiology*, 2003, **149**, 2005–2013.
31 S. Wilhelm, A. Gdynia, P. Tielen, F. Rosenau and K.-E. Jaeger, The Autotransporter Esterase EstA of Pseudomonas aeruginosa Is Required for Rhamnolipid Production, Cell Motility, and Biofilm Formation, *J. Bacteriol.*, 2007, **189**, 6695–6703.
32 A. A. Bodour, K. P. Drees and R. M. Maier, Distribution of biosurfactant-producing bacteria in undisturbed and contaminated arid southwestern soils, *Appl. Environ. Microbiol.*, 2003, **69**, 3280–3287.
33 S. Al Shamaa and S. Bahjat, Detection of Rhamnolipid Production in Pseudomonas aeruginosa, *J. Phys.: Conf. Ser.*, 2019, **1294**, 062083.
34 D. P. Cassidy, A. J. Hudak, D. D. Werkema, E. A. Atekwana, S. Rossbach, J. W. Duris, E. A. Atekwana and W. A. Sauck, In situ rhamnolipid production at an abandoned petroleum refinery, *Soil Sediment Contam.*, 2002, **11**, 769–787.
35 A. J. Hudak and D. P. Cassidy, Stimulating in-soil rhamnolipid production in a bioslurry reactor by limiting nitrogen, *Biotechnol. Bioeng.*, 2004, **88**, 861–868.
36 F. Zhao, P. Li, C. Guo, R. J. Shi and Y. Zhang, Bioaugmentation of oil reservoir indigenous Pseudomonas aeruginosa to enhance oil recovery through in-situ biosurfactant production without air injection, *Bioresour. Technol.*, 2018, **251**, 295–302.
37 C. Liu, Y. Zhang, S. Sun, L. Huang, L. Yu, X. Liu, R. Lai, Y. Luo, Z. Zhang and Z. Zhang, Oil recovery from tank bottom sludge using rhamnolipids, *J. Pet. Sci. Eng.*, 2018, **170**, 14–20.
38 Z. Sahebnazar, D. Mowla, G. Karimi and F. Yazdian, Zero-valent iron nanoparticles assisted purification of rhamnolipid for oil recovery improvement from oily sludge, *J. Environ. Chem. Eng.*, 2018, **6**, 917–922.
39 C. J. Boxley, J. E. Pemberton and R. M. Maier, Rhamnolipids and related biosurfactants for cosmetics and cosmeceutical markets, *Int. News Fats, Oils Relat. Mater.*, 2015, **26**, 206–215.
40 T. Cheng, J. Liang, J. He, X. Hu, Z. Ge and J. Liu, A novel rhamnolipid-producing Pseudomonas aeruginosa ZS1 isolate derived from petroleum sludge suitable for bioremediation, *AMB Express*, 2017, **7**, 120.
41 W. Li, C. H. Hinton, S. S. Lee, J. Wu and J. D. Fortner, Surface engineering superparamagnetic nanoparticles for aqueous applications: Design and characterization of tailored organic bilayers, *Environ. Sci.: Nano*, 2016, **3**, 85–93.
42 W. Li, S. Lee, J. Wu, C. H. Hinton and J. D. Fortner, Shape and size controlled synthesis of uniform iron oxide nanocrystals through new non-hydrolytic routes, *Nanotechnology*, 2016, **27**, 324002.
43 J. D. Clogston and A. K. Patri, Zeta potential measurement, in *Characterization of Nanoparticles Intended for Drug Delivery, Methods in Molecular Biology*, ed. S. McNeil, Humana Press, 2011, vol. 697, pp. 63–70.
44 S. Skoglund, J. Hedberg, E. Yunda, A. Godymchuk, E. Blomberg and I. O. Wallinder, Difficulties and flaws in performing accurate determinations of zeta potentials of metal nanoparticles in complex solutions—Four case studies, *PLoS One*, 2017, **12**, e0181735.
45 D. R. Perinelli, M. Cespi, N. Lorusso, G. F. Palmieri, G. Bonacucina and P. Blasi, Surfactant Self-Assembling and Critical Micelle Concentration: One Approach Fits All?, *Langmuir*, 2020, **36**, 5745–5753.
46 H. Zhong, G. M. Zeng, J. X. Liu, X. M. Xu, X. Z. Yuan, H. Y. Fu, G. H. Huang, Z. F. Liu and Y. Ding, Adsorption of monorhamnolipid and dirhamnolipid on two Pseudomonas aeruginosa strains and the effect on cell surface hydrophobicity, *Appl. Microbiol. Biotechnol.*, 2008, **79**, 671–677.
47 S. K. Nandwani, M. Chakraborty and S. Gupta, Adsorption of Surface Active Ionic Liquids on Different Rock Types under High Salinity Conditions, *Sci. Rep.*, 2019, **9**, 1–16.
48 H. Holthoff, S. U. Egelhaaf, M. Borkovec, P. Schurtenberger and H. Sticher, Coagulation Rate Measurements of Colloidal Particles by Simultaneous Static and Dynamic Light Scattering, *Langmuir*, 1996, **12**, 5541–5549.
49 S. E. Mylon, K. L. Chen and M. Elimelech, Influence of Natural Organic Matter and Ionic Composition on the Kinetics and Structure of Hematite Colloid Aggregation: Implications to Iron Depletion in Estuaries, *Langmuir*, 2004, **20**, 9000–9006.
50 B. Derjaguin and L. Landau, Theory of the stability of strongly charged lyophobic sols and of the adhesion of strongly charged particles in solutions of electrolytes, *Prog. Surf. Sci.*, 1993, **43**, 30–59.
51 E. J. W. Verwey and J. T. G. Overbeek, Theory of the stability of lyophobic colloids, *J. Colloid Sci.*, 1955, **10**, 224–225.
52 W. B. Russel, D. A. Saville and W. R. Schowalter, *Colloidal Dispersions*, Cambridge University Press, 1st edn, 1990.
53 M. Li and M. Kobayashi, The aggregation and charging of natural clay allophane: Critical coagulation ionic strength in the presence of multivalent counter-ions, *Colloids Surf., A*, 2021, **626**, 127021.
54 G. Trefalt, I. Szilagyi, G. Téllez and M. Borkovec, Colloidal stability in asymmetric electrolytes: Modifications of the Schulze–Hardy rule, *Langmuir*, 2017, **33**, 1695–1704.
55 Z. Tian, M. Li, T. Sugimoto and M. Kobayashi, The Effect of Lysozyme on the Aggregation and Charging of Oxidized Carbon Nanohorn (CNHox) in Aqueous Solution, *Appl. Sci.*, 2024, **14**, 2645.
56 H. M. Qin, D. Gao, M. Zhu, C. Li, Z. Zhu, H. Wang, W. Liu, M. Tanokura and F. Lu, Biochemical characterization and structural analysis of ulvan lyase from marine Alteromonas sp. reveals the basis for its salt tolerance, *Int. J. Biol. Macromol.*, 2020, **147**, 1309–1317.
57 A. Javed, F. Steinke, S. Wöhlbrandt, H. Bunzen, N. Stock and M. Tiemann, The role of sulfonate groups and hydrogen bonding in the proton conductivity of two coordination networks, *Beilstein J. Nanotechnol.*, 2022, **13**, 437–443.
58 S. Peker, Ş. Helvaci and G. Özdemir, Interface–Subphase Interactions of Rhamnolipids in Aqueous Rhamnose Solutions, *Langmuir*, 2003, **14**, 5838–5845.
59 S. Skoglund, E. Blomberg, I. O. Wallinder, I. Grillo, J. S. Pedersen and L. M. Bergström, A novel explanation for the enhanced colloidal stability of silver nanoparticles in the

presence of an oppositely charged surfactant, *Phys. Chem. Chem. Phys.*, 2017, **19**, 28037–28043.
60 F. Loosli, P. Le Coustumer and S. Stoll, TiO2 nanoparticles aggregation and disaggregation in presence of alginate and Suwannee River humic acids. pH and concentration effects on nanoparticle stability, *Water Res.*, 2013, **47**, 6052–6063.
61 D. Song, Y. Li, S. Liang and J. Wang, Micelle behaviors of sophorolipid/rhamnolipid binary mixed biosurfactant systems, *Colloids Surf., A*, 2013, **436**, 201–206.
62 A. I. Rodrigues, E. J. Gudiña, J. A. Teixeira and L. R. Rodrigues, Sodium chloride effect on the aggregation behaviour of rhamnolipids and their antifungal activity, *Sci. Rep.*, 2017, **7**, 1–9.
63 H. Wang, X. Zhao, X. Han, Z. Tang, S. Liu, W. Guo, C. Deng, Q. Guo, H. Wang, F. Wu, X. Meng and J. P. Giesy, Effects of monovalent and divalent metal cations on the aggregation and suspension of Fe3O4 magnetic nanoparticles in aqueous solution, *Sci. Total Environ.*, 2017, **586**, 817–826.
64 K. L. Chen, S. E. Mylon and M. Elimelech, Enhanced aggregation of alginate-coated iron oxide (Hematite) nanoparticles in the presence of calcium, strontium, and barium cations, *Langmuir*, 2007, **23**, 5920–5928.
65 G. Trefalt, I. Szilágyi and M. Borkovec, Schulze-Hardy rule revisited, *Colloid Polym. Sci.*, 2020, **298**, 961–967.
66 S. S. Helvac, S. Peker and G. Özdemir, Effect of electrolytes on the surface behavior of rhamnolipids R1 and R2, *Colloids Surf., B*, 2004, **35**, 225–233.
67 A. A. Keller, H. Wang, D. Zhou, H. S. Lenihan, G. Cherr, B. J. Cardinale, R. Miller and Z. Ji, Stability and Aggregation of Metal Oxide Nanoparticles in Natural Aqueous Matrices, *Environ. Sci. Technol.*, 2010, **44**, 1962–1967.
68 T. Abe, S. Kobayashi and M. Kobayashi, Aggregation of colloidal silica particles in the presence of fulvic acid, humic acid, or alginate: Effects of ionic composition, *Colloids Surf., A*, 2011, **379**, 21–26.